telecom

MDPI

Article

Fifth-Generation (5G) Communication in Urban Environments: A Comprehensive Unmanned Aerial Vehicle Channel Model for Low-Altitude Operations in Indian Cities

Ankita K. Patel * and Radhika D. Joshi

Department of Electronics and Telecommunication Engineering, College of Engineering Pune Technical University, Pune 411005, India; rdj.extc@coeptech.ac.in
* Correspondence: ankitaketan@gmail.com; Tel.: +91-940-4239-178

Abstract: Unmanned aerial vehicles (UAVs) significantly shape the evolution of 5G and 6G technologies in India, particularly in reconfiguring communication networks. Through their deployment as base stations or relays, these aerial vehicles substantially enhance communication performance and extend network coverage in areas characterized by high demand and challenging topographies. Accurate modelling of the UAV-to-ground channel is imperative for gaining valuable insights into UAV-assisted communication systems, particularly within India's rapidly expanding metropolitan cities and their diverse topographical complexities. This study proposes an approach to model low-altitude channels in urban areas, offering specific scenarios and tailored solutions to facilitate radio frequency (RF) planning for Indian metropolitan cities. The proposed model leverages the International Telecommunication Union recommendation (ITU-R) for city mapping and utilizes frequency ranges from 1.8 to 6 GHz and altitudes up to 500 m to comprehensively model both line-of-sight (LoS) and non-line-of-sight (NLoS) communications. It employs the uniform theory of diffraction to calculate the additional path loss for non-line-of-sight (NLoS) communication for both vertical and horizontal polarizations. The normal distribution for additional shadowing loss is discerned from simulation results. This study outlined the approach to derive a comprehensive statistical channel model based on the elevation angle and evaluate model parameters at various frequencies and altitudes for both vertical and horizontal polarization. The model was subsequently compared with existing models for validation, showing close alignment. The ease of implementation and practical application of this proposed model render it an invaluable tool for planning and simulating mobile networks in urban areas, thus facilitating the seamless integration of advanced communication technologies in India.

Keywords: UAV; low altitude; ITU-R Model; 5G communication; uniform theory of diffraction

Academic Editor: Mario E. Rivero-Angeles

Received: 14 December 2024
Revised: 16 January 2025
Accepted: 22 January 2025
Published: 4 February 2025

Citation: Patel, A.K.; Joshi, R.D. Fifth-Generation (5G) Communication in Urban Environments: A Comprehensive Unmanned Aerial Vehicle Channel Model for Low-Altitude Operations in Indian Cities. *Telecom* **2025**, *6*, 9. https://doi.org/10.3390/telecom6010009

1. Introduction

The advent of the fifth generation (5G) of communications can revolutionize services by providing enhanced end user experiences, seamless coverage, high data rates, and low latency, thus significantly improving performance and reliable communications [1]. The rollout of 5G services in India began in October 2022 and will expand across 28 states and eight union territories by 2024. According to Ericsson's projections, the number of 5G users in India is expected to reach 700 million by the end of 2028 [2]. This technology is anticipated to play a pivotal role in achieving the goals of the Digital India Program established by the Government of India. The launch of 5G services in India faces several challenges, primarily the need to fundamentally redesign the communication system's core architecture. Unlike 4G, 5G struggles with long-distance data transmission, necessitating a denser network with small cell architecture—consisting of numerous low-power base stations for better coverage. This shift demands significant infrastructure investments, including more cell towers and improved supporting technologies to fully leverage 5G's capabilities and ensure seamless connectivity nationwide. Implementing this advanced infrastructure demands substantial investments in additional cell towers and supporting technologies to maximize 5G's potential.

To overcome these obstacles, unmanned aerial vehicles (UAVs) present a promising solution, particularly within India's rapidly evolving metropolitan landscapes. As cities expand geographically, UAVs can function as dynamic aerial base stations, relays, or aerial servers [3–5]. We can significantly enhance communication performance and coverage by integrating these flying machines with existing base stations. This synergy facilitates improved data transmission and extends the reach of 5G networks, ultimately paving the way for a robust and interconnected future. UAV base stations are distinct from UAVs primarily due to their advanced communication infrastructure. Unlike UAVs, which may lack a dedicated communication system, UAV base stations—often referred to as drone base stations or flying base stations—are specifically designed to enhance connectivity. These stations are equipped with essential components such as antennas, transceivers, and power supplies, enabling them to establish reliable communication with ground users effectively. This robust setup allows for seamless data transfer, real-time monitoring, and improved operational efficiency in various applications, including surveillance, mapping, and emergency response.

Furthermore, incorporating UAVs with wireless sensor networks can support various applications, such as agriculture, surveys, package and food delivery, aerial photography, etc. [6,7]. UAVs will be invaluable in emergency and public safety scenarios in which the terrestrial network is compromised. By deploying UAVs with communication systems, authorities can establish temporary networks to coordinate rescue efforts and relay vital information [8].

The deployment of UAVs as base stations or communication relays necessitates a thorough assessment of the communication infrastructure requirements for effective service establishment. This consideration is particularly crucial given the limited energy capacity of UAVs. To achieve a successful network deployment, it is vital to determine several key factors: the optimal number of base stations required, the operational altitude for the UAVs, and the specific level of service expected by users. When UAVs are utilized for air-to-ground communication at low altitudes—essentially mirroring traditional cellular network principles—efficient deployment becomes increasingly paramount. A robust and precise channel model is essential in this context, as it provides the foundation for accurately calculating path loss and power consumption. By carefully analyzing these technical variables, operators can ensure that their network will provide adequate coverage and service quality across targeted geographic regions, ultimately enhancing user experience and operational reliability.

The impetus behind this proposal arises from two crucial factors that significantly impact the development of communication models in Indian metropolitan cities: (i) the current lack of a comprehensive generalized model that encompasses all urban environments within these cities; (ii) the necessity for a singular model that effectively captures the interplay between essential elements of UAV communication such as polarization, altitude, elevation, and frequency. In light of the absence of established models that address low-altitude UAV links—particularly those influenced by shadowing loss components—this proposal aims to introduce a generalized channel model for UAV communication. This initiative is especially pertinent for Indian metropolitan cities, which need advanced communication infrastructures to support the rollout of 5G technology.

The urban fabric of Indian metropolitan cities can be distinctly categorized into four environmental scenarios: (i) the suburban environment, which encompasses the extended city peripheries that have characteristics akin to rural areas; (ii) the urban environment, representing any typical area within the city; (iii) the dense urban environment, characterized by closely clustered buildings and limited open spaces; and (iv) the high-rise urban environment, highlighting newly developed regions featuring skyscraper-style architecture. These varied urban settings necessitate the development of a channel model to accurately assess path loss and shadowing variations at different heights. Presently, established generalized models relying on statistical parameters from ITU-R P.1410-5 fall short of addressing low altitudes below 500 m, requiring many applications associated with 5G communication. Deploying low-altitude systems ensures that devices stay within close range, leading to more reliable data connections. This proximity enhances connection quality, allowing for stable transmissions and seamless connectivity, even in densely populated areas where device saturation is an issue. A robust and comprehensive channel model is essential for integrating UAVs as aerial base stations into the existing ground station infrastructure. This model should consider diverse scenarios, frequency ranges, and altitudes pertinent to urban communication. This paper focuses on constructing a model that reflects the four identified scenarios within Indian metropolitan cities while aligning with the frequency and altitude requirements specific to 5G technology. The key contributions of this paper are multifaceted:

1. A statistical model is proposed to predict the link between the UAV (transmitter) and the end users (receivers).
2. The proposed model is based on ITU-R statistical parameters for city layout and the uniform theory of diffraction to account for additional path loss.
3. The additional path loss is mapped with a normal distribution, and distribution parameters are assessed.
4. The model's formulation depends on the elevation angle, and its parameters are computed for different frequencies and altitudes, considering both vertical and horizontal polarization.
5. The proposed model is compared with existing models for validation.
6. The impact of variation in frequency and UAV altitude on path loss is discussed.

Through this comprehensive approach, we aim to provide a significant contribution to the field of urban communication infrastructure, enabling better integration of UAV technology within the context of 5G networks in India.

This paper's propagation model is established on simulations conducted in a randomly generated urban environment. This paper is structured as follows: Section 2 overviews air-to-ground channel modelling. Section 3 presents a simulation of a city featuring four environments, which represent Indian metropolitan cities. In Sections 4 and 5, a new model is proposed and subjected to analysis, followed by validation of the model in Section 6. Finally, Section 7 offers concluding remarks on this study.

2. Air to Ground Channel Modelling

Two primary methods are utilized for categorizing the air-to-ground channel: an empirical channel based on measurement data and a deterministic or geometry-based channel model derived from simulated data [9].

The empirical channel model used measurement data for C-band- and L-band-using aircraft in scenarios like suburban, urban, over-water, hilly, and mountainous environments [10–13]. The data provided by measurement gives insight into the statistical properties of different terrains. In [14], the authors investigated the impact of airframe shadowing on the channel. They also provided a solution to mitigate this effect by effectively deploying multiple antennas. The statistical properties of large-scale and small-scale fading were analyzed using measurements for suburban areas, rural areas, and open areas of a city in the context of air-to-ground UAV communication, as detailed in [15,16]. Determination of path loss for low-altitude UAV channels at frequencies 2.4 and 5.9 GHz was achieved by using a multilink measurement campaign [17]. The authors proposed path loss based on elevation angle and distance and further analyzed the shadow fading across different frequency bands and evaluated spatial correlations. A medium-sized UAV conducted low-altitude measurements in a suburban area to investigate multipath effects [18]. In Reference [19], the authors used a fixed-wing UAV for an air-to-ground channel measurement campaign conducted at low altitudes in a rural area, at 2.7 GHz. The paper offers details about the measurement system and analysis of large-scale fading, including path loss, shadow fading, and small-scale fading. The UAV provided a path loss model and identified the impact of altitude on the channel. While measurement data offer firsthand insights into channel characteristics, it is essential to note that such data are site-specific and may not be broadly applicable to general scenarios. Furthermore, specific measurement environments are complex and involve high costs.

The deterministic channel modelling approach using ray tracing can demonstrate the channel's performance when considering environmental conditions. A ray tracing method was used to characterize a propagation channel model for rural, suburban, and dense urban scenarios at 28 GHz to find the effect of multipath components at the receiver [20]; suburban open-environment channel characteristics are analyzed in [21]. A ray tracing-based Monte Carlo method was used to analyze and evaluate UAV air-to-ground channel model performance [22]. Geometry-based stochastic models are widely used to evaluate spatial and temporal variation and characterize air-to-ground channels. A regular-shaped, geometry-based stochastic model for a UAV MIMO channel is proposed in [23]. The statistical characteristics of the channel were ascertained by considering parameters such as altitude and flight movement. A model with mixed bouncing was proposed to capture AG channel characteristics [24]. Taking into consideration the changing moving direction and speed of the MS, a channel model of 3D wideband MIMO was proposed [25], and the statistical properties were verified by simulation data and theoretical data. The models are tailored to specific geometries and unsuitable for different scenarios. A multi-UAV OFDMA communication system that utilizes geographical information develops a realistic channel model incorporating blockage-aware parameters [26].

In the existing body of literature, generic models are available to determine statistical parameters for modelling the UAV air-to-ground channel [27–33]. In [27], the authors introduce a generic statistical model tailored for low-altitude platforms, where the channel model parameters are derived via 3D ray-tracing at frequency bands of 700, 2000, and 5800 MHz for altitudes up to 2 km. Furthermore, the probability of the line-of-sight (LoS) channel of a UAV is modelled utilizing a sigmoid function of the vertical angle between the UAV and the user, as presented in [28]. This model is leveraged to characterize the coverage radius for an aerial base station of the UAV as a function of path loss, alongside assessments of the optimal UAV altitude in [29,30]. The WIRELESS Insite software version 2.5, program is employed to simulate a dense urban environment at varying altitudes and frequencies, further refined through analytical formulation using the knife edge refraction model [31]. A statistical model specific to high altitude, based on elevation, is delineated in [32]. The methodology for estimating coverage using the generalized UAV air-to-ground channel model for altitudes up to 100 m is explained in [33]. In comparison, for altitudes up to 500 m, it is delineated in [34]. Authors in [35] furnish a comprehensive channel model for UAV linkages based on the alpha-beta model framework.

The existing body of literature concerning the generic channel model does not sufficiently investigate low-altitude communication links for unmanned aerial vehicles (UAVs) within the complex and varied urban landscapes of India. Previous research underscores the critical need for an elevation-based model, which can improve the precision of path loss calculations and account for shadowing variations that occur at different altitudes. The objective of this study is to introduce a comprehensive air-to-ground channel model that takes elevation angles into account. This model will utilize statistical parameters recommended by the International Telecommunication Union (ITU-R), specifically tailored to suit various environments, including suburban, urban, dense urban, and high-rise urban areas. By doing so, this study aims to support the effective expansion and implementation of 5G communication systems across the diverse urban settings in India. The proposed system aims to enhance the coverage area while managing the energy requirements of UAVs operating as aerial base stations (ABSs). It incorporates power reduction techniques such as trajectory optimization through efficient flight planning, flexible user assignment to nearby base stations, and dynamic adjustment of the coverage area based on demand. These strategies are designed to address the limited energy capacity of UAVs.

3. Modeling of City Environment

The building's layout and characteristics significantly impact the radio frequency (RF) model in an urban setting. These factors include building heights, materials, spacing between buildings, and obstacles such as trees and other structures. Understanding these conditions and constraints is essential for accurately developing an RF model to account for signal propagation and coverage in urban areas effectively. The statistical ITU-R recommendation P.1410-5 [36] model allows for us to create the build-up area for an urban environment without specific information about building shapes and distribution. As per [34], only three parameters are needed to model the area: α, which is the ratio of build-up area to the total land area (dimensionless); β, the mean number of buildings per unit area (buildings/km^2); γ, a scale parameter that describes the distribution of building heights according to a Rayleigh probability density function.

$$p(h_b) = \frac{h_b}{\gamma^2}\ \exp(\frac{-{h_b}^2}{\gamma^2}) \tag{1}$$

where $p(h_b)$ is the probability distribution of the building with height h_b.

The statistical ITU-R model parameters are utilized to create four different environments that can be used to map the area of an Indian metropolitan city. Table 1 summarizes the above-mentioned statistical parameters based on ITU-R recommendation P.1410-5 [36]. These parameters are utilized to create four distinct environments that can be correlated with urban areas. The distribution of buildings is generated using the Rayleigh distribution to ensure a realistic approach when analyzing shadowing effects.

Table 1. ITU-R P.1410-5 model parameters.

Environment	**α**	**β**	**Γ**
Suburban	0.1	750	8
Urban	0.3	500	15
Dense urban	0.5	300	20
High-rise urban	0.5	300	50

Designing a geometric model that meets these criteria to represent an acceptable city layout is a significant challenge. This paper utilizes a mathematical approximation proposed by Al Hurani [27] to shape the city environment, as shown in Figure 1. The simulation considers a square plot with an area of one square kilometer, where the total number of buildings is Ns, the side length is denoted as Ds, the building width is Ws, and the interbuilding space is Ss, all measured in meters. As per [27], the ITU-R statistical parameters can be linked with D_s, W_s, and S_s with the relationship $W_s = 1000\sqrt{\frac{\alpha}{\beta}}$, with interbuilding spacing $S_s = \frac{1000}{\sqrt{\beta}} - W_s$ and side length $D_s = \frac{W_s+S_s}{1000}\sqrt{N_s}$.

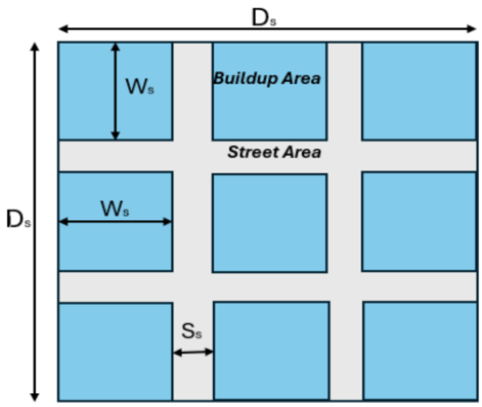

Figure 1. Selected layout for city areas.

The city layout can be easily generated using MATLAB 2023. In the real-world environment, buildings do not have a regular structure. To mitigate that in simulation, the UAV's position is determined by the elevation and azimuthal angles at each point along the street. Calculations are carried out for specific elevation angles using the median value obtained from the azimuthal angle. This approach ensures that the results are not dependent on the azimuthal angle, accounting for the uneven spacing of buildings in the real world.

Simulation Method

The simulation is performed using MATLAB. It is divided into two parts: The first is that LoS probability in the street is studied as a function of elevation angle for four types of build areas. Second, the additional path loss resulting from the shadowing effects of buildings is investigated using the uniform theory of diffraction (UTD) method [35,36]. Our analysis considers the building's walls constructed of concrete and brick with relative permittivity ε of 15 and 4, respectively and conductivity σ (0.015 S/m). Diffraction loss for vertical and horizontal polarization is computed separately. Figure 2 shows the geometry that encompasses both LoS and NLoS communication.

The simulation involves creating four virtual environments within a 1 km × 1 km area to mimic different scenarios in MATLAB. The UAV's position is determined along the street. The azimuthal angle ranges from 0 to 360 degrees in increments of 9 degrees. Calculations are carried out for specific elevation angles using the median value obtained from the azimuthal angle. This approach ensures that the results are not dependent on the azimuthal angle, accounting for the uneven spacing of buildings in the real world. The simulation covers elevation angles from 1 to 89 degrees, assuming a maximum UAV altitude of 500 m. This setup reflects the use of the UAV as a base station or relay to meet the demand of 5G and beyond.

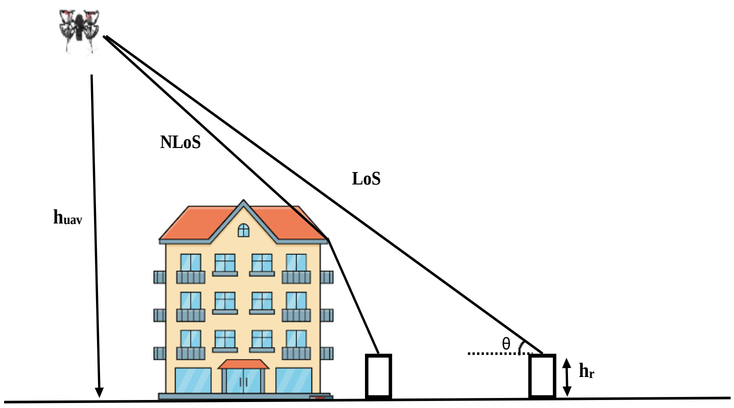

Figure 2. Geometry of LoS and NLoS scenario.

4. New Propagation Model

The simulation results are categorized into two distinct components: the first pertains to the LoS probability on the street; the FSPL model is applicable for calculating the average propagation loss and the second is additional path loss due to the shadowing effect of propagation buildings for NLoS conditions. Our previous investigation [34] shows that an elevation angle of 60 to 80 degrees provides the most realistic coverage area. However, it is also important to consider other elevation angles, as they may be significant for studying interference and other related factors.

4.1. Modelling Line of Sight Probability

The LoS probability on the street is obtained based on elevation angle for four environments with UAV altitudes up to 500 m and azimuthal angles between 0 and 360 degrees. The LoS probability proposed in our previous work [34] is given by

$$P_{LoS} = \frac{1}{a_3 + e^{-(-a_1 + a_2(\theta - a_4))}} \tag{2}$$

where a_1, a_2, a_3, and a_4 are the empirical parameters. The empirical parameter values for the suburban environment are (2.1778, 0.3557, 1, 0), the urban environment (3.0734, 0.1565, 0.9989, 0.158), the dense urban environment (3.4912, 0.1304, 1.007, 0.3344), the high-rise urban environment below elevation angle 45 degrees (4.2234, 0.8815, 1.5747, 0.114), and the high-rise urban environment above elevation angle 45 degrees (4.7313, 0.1209, 0.9801, 13.144).

4.2. Shadowing Loss

The analysis of additional path loss resulting from the shadowing effect of buildings using the uniform theory of diffraction (UTD) [37–39] and the method outlined in ITU-R P.526-14 for diffraction-based propagation using UTD [40]. This methodology applies to both vertical and horizontal polarizations to predict diffraction loss induced by a finitely conducting wedge. It is pertinent in diffraction scenarios around building corners, across terrain featuring a wedge-shaped hill, or over roof ridges. The method requires the conductivity and relative dielectric constant of the obstructing wedge and assumes that no transmission occurs through the wedge material. Furthermore, the method accounts for diffraction in both shadow and line-of-sight regions, facilitating a smooth transition between these zones. Figure 3 visualizes the geometry associated with wedge diffraction as delineated by UTD.

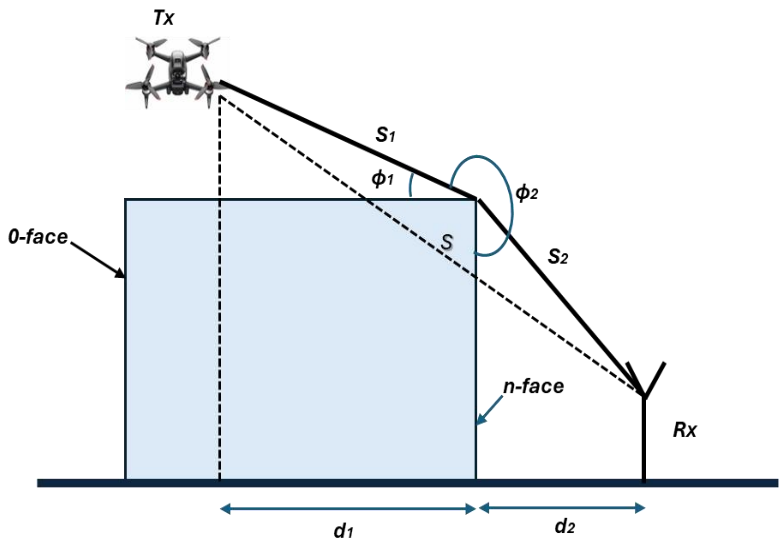

Figure 3. Geometry of wedge diffraction.

The UTD formulation for the electric field at the field point:

$$E_{UTD} = E_0 \frac{e^{-jk(s_1+s_2)}}{s_1} D \sqrt{\frac{s_1}{s_2(s_1+s_2)}} \tag{3}$$

where E_{UTD} is the electric field at the field point; E_0 is relative source amplitude, s_1 and s_2 are distanced from the source point to the diffracting edge and the diffracting edge to the field point, respectively; k is the wave numberz; D is the diffraction coefficient depending on the polarization (parallel or perpendicular to the plane of incidence) of the incident field on edge; (refer to [39] for formulas of D for vertical and horizontal polarization); and s is the distance between transmitter and receiver with obstruction. The relative field strength at the field point to the field in the absence of the obstruction is

$$E_{UTD}(dB) = 20\log\left(\left|\frac{sE_{UTD}}{e^{-jks}}\right|\right) \tag{4}$$

The relative diffraction loss based on UTD model is

$$L_{UTD} = 20\log\left(\frac{\sqrt{s_1 s_2(s_1+s_2)}}{s|D|}\right) \tag{5}$$

This simulation study explores the diffraction loss experienced in various environmental contexts by examining vertical and horizontal polarization. The calculations are conducted at an elevation angle of 70 degrees, a frequency of 2.1 GHz, and an altitude of 200 m across four distinct environments: suburban, urban, dense urban, and high-rise.

The normalized histogram of the diffraction loss is presented in Figure 4a–d. The histogram indicates that the distribution of loss values closely resembles a normal distribution. It was observed that the histogram aligns well with this pattern. To further support this finding, the probability density function (pdf) of the normal distribution is fitted to the simulated data, as shown in Figure 4. This fitting highlights the consistency of the diffraction loss across different environments, thereby enhancing the credibility of the simulation results. The pdf of the normal distribution is given by

$$p(z) = \frac{1}{\sigma\sqrt{2\pi}} e^{-\left(\frac{(x-\mu)^2}{2\sigma^2}\right)} \tag{6}$$

where p is the normalized probability, μ is the mean value in dB, and σ is the standard deviation. Table 2 gives the normal distribution's mean and standard deviation.

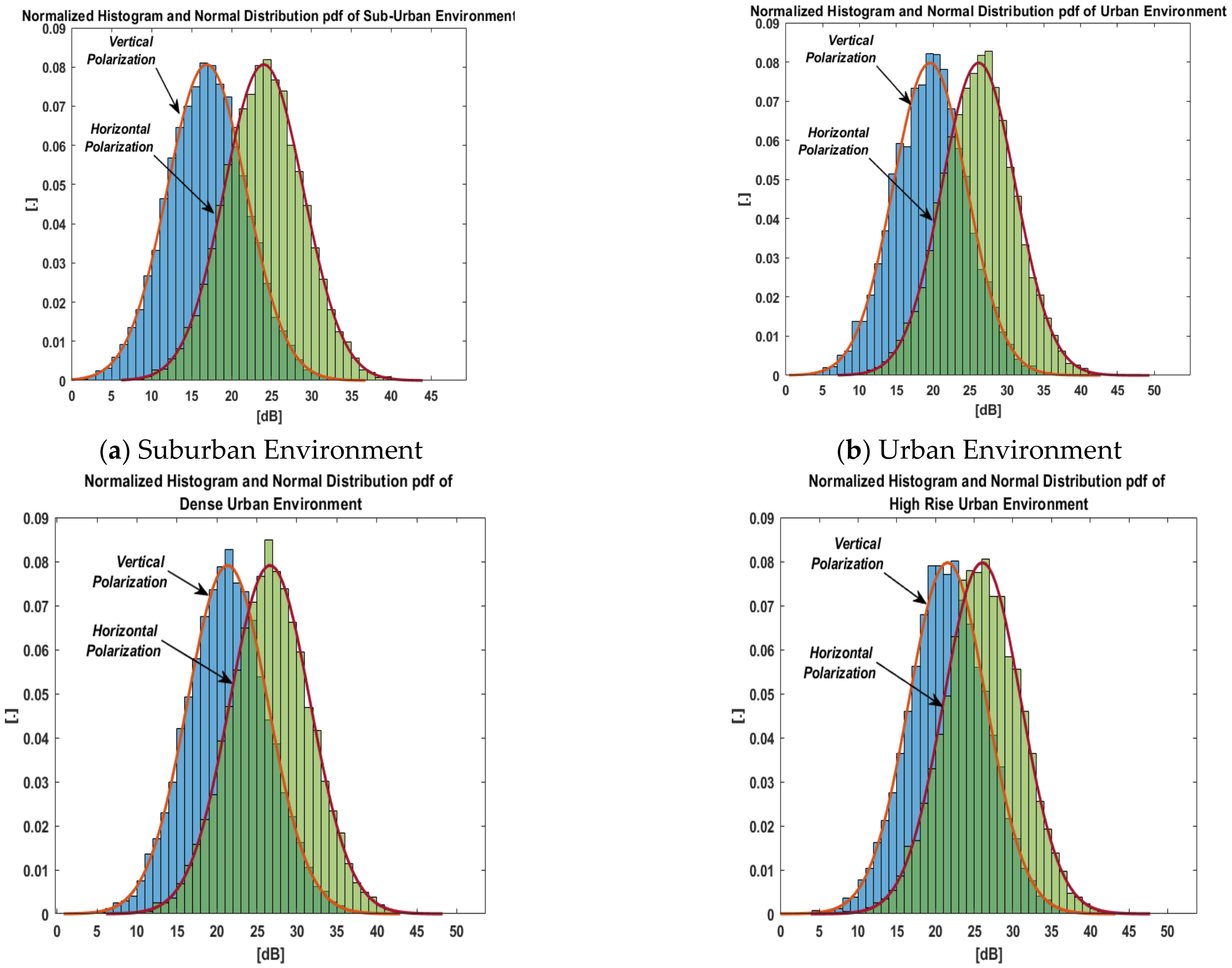

(**a**) Suburban Environment (**b**) Urban Environment

(**c**) Dense-urban Environment (**d**) High-rise-urban Environment

Figure 4. (**a**–**d**) Normalized histogram of shadowing loss at 2.1 GHz for elevation angle 70°.

Table 2. Mean and variance of normal distribution at 70 degrees and frequency 2.1 GHz.

Environment	Vertical		Horizontal	
	Mean(dB)	Standard Deviation (dB)	Mean(dB)	Standard Deviation (dB)
Suburban	16.8603	5.0019	23.9999	5.0019
Urban	19.5104	5.0119	26.1119	5.0119
Dense Urban	21.3564	5.0124	26.6517	5.0124
High-Rise urban	16.5303	5.0136	21.0535	5.0136

Further, the cumulative distribution function (CDF) of vertical and horizontal polarization across all environments is simulated for elevation angles ranging from 10 to 80 degrees, as illustrated in Figure 5. The dashed curve in the figure denotes the CDF of the normal distribution of the simulated data. The close correspondence between the simulated data and the normally distributed data is evident from the figure. The graph demonstrates that the CDF for elevation angles between 10° and 40° is nearly identical for vertical polarization, whereas this is not the case for horizontal polarization. Here, altitudes range from 100 to 500 m.

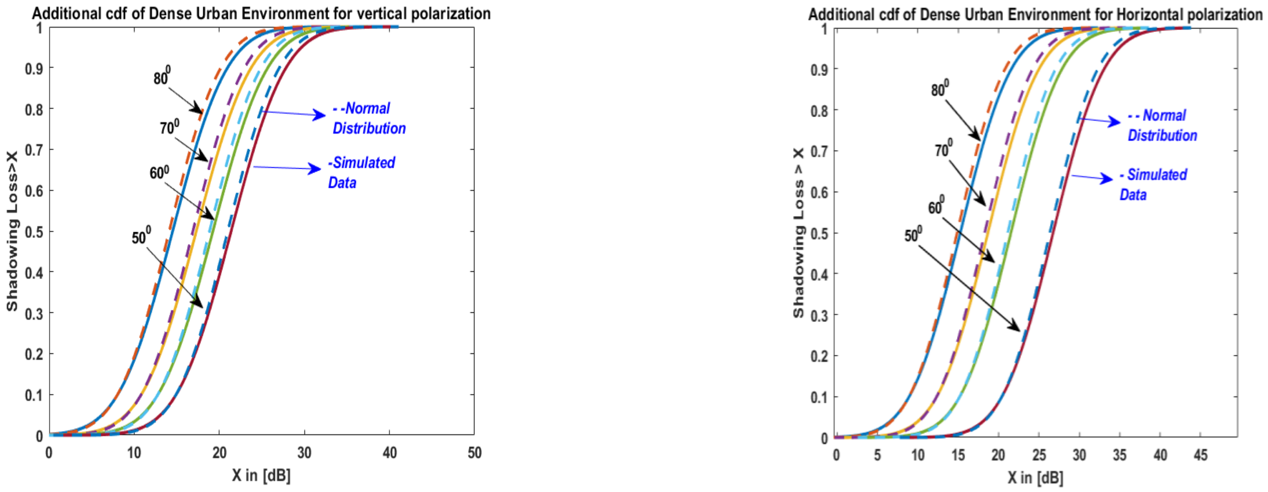

Figure 5. CDF of shadowing loss for horizontal and vertical polarization at 2.1 GHz for dense urban environment.

These revealed a significant increase in shadowing loss at these higher frequencies and altitudes. Figures 6 and 7 show the parameters of a normal distribution mean and standard deviation for three different carrier frequencies and elevation angles ranging from 1 to 89 degrees across all four environmental scenarios, considering a UAV altitude of 200 m. A rational function was developed to effectively model the mean of a normal distribution, while a linear function was used to represent the standard deviation based on the simulation results depicted in Figures 4 and 5. Equation (7) approximates the normal distribution's mean value, and Equation (8) approximates the standard deviation.

$$\mu = \frac{p_1\theta + p_2}{\theta + p_3} \tag{7}$$

$$\sigma = s_1\theta + s_2 \tag{8}$$

where θ is the elevation angle in degrees; p_1, p_2, and p_3 are empirical parameters for the mean; and s_1, s_2 are for standard deviation.

An extensive series of experiments was conducted to analyze communication dynamics at various altitudes, ranging from 100 m to 500 m, reflecting the height of base stations in an Indian city. The frequencies examined during this research are 1.8 GHz, 2.1 GHz, and 5.8 GHz, frequencies used by many operators in India. The objective was to accurately model the mean and standard deviation of a normal distribution associated with these parameters. This study focused on both vertical and horizontal polarizations, and it was carried out under a wide range of environmental conditions, ensuring that the findings would be robust and applicable in real-world scenarios.

The results of our extensive experimentation provide valuable insights into the empirical parameters of the means and standard deviations of the normal distribution as per Equations (7) and (8), which are systematically presented in Tables 3–5. Within Tables 3 and 4, we identify empirical parameters labeled p_1, p_2, and p_3. These parameters reflect the mean values obtained from our rigorous experimental processes, showcasing the central tendencies across different conditions.

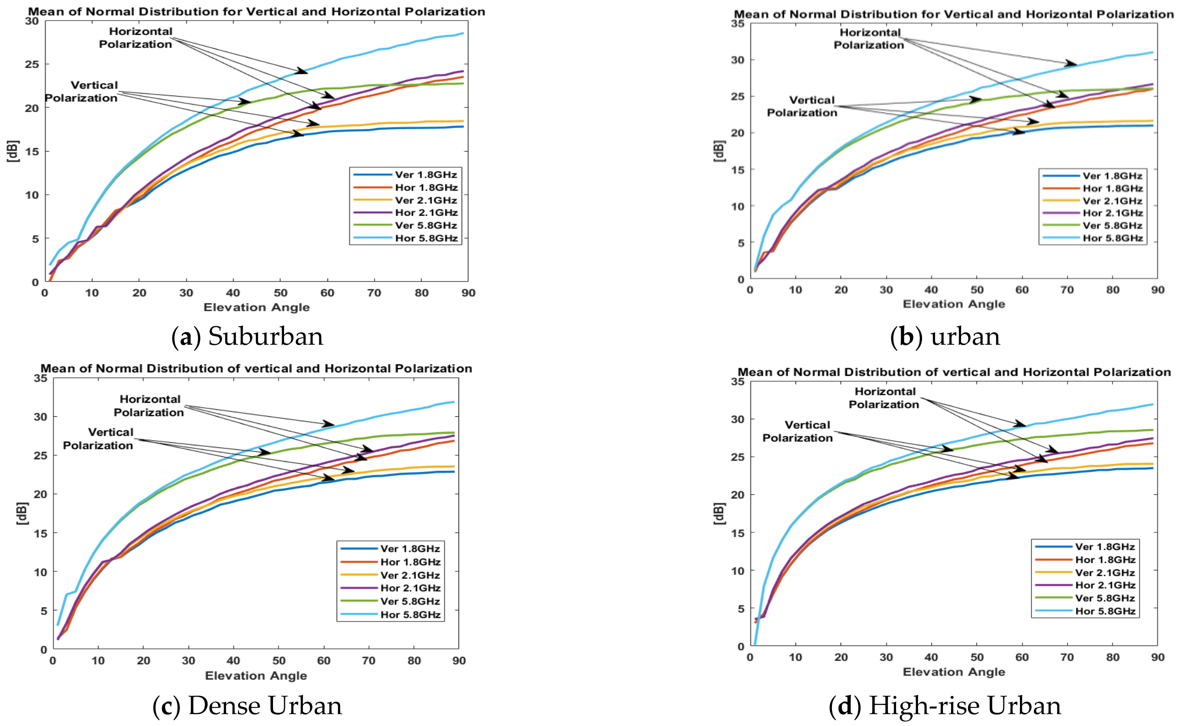

Figure 6. (**a**–**d**) mean of normal distribution for horizontal and vertical polarization at 1.8 GHz, 2.1 GHz, and 5.8 GHz for different environments for a range of elevation angles.

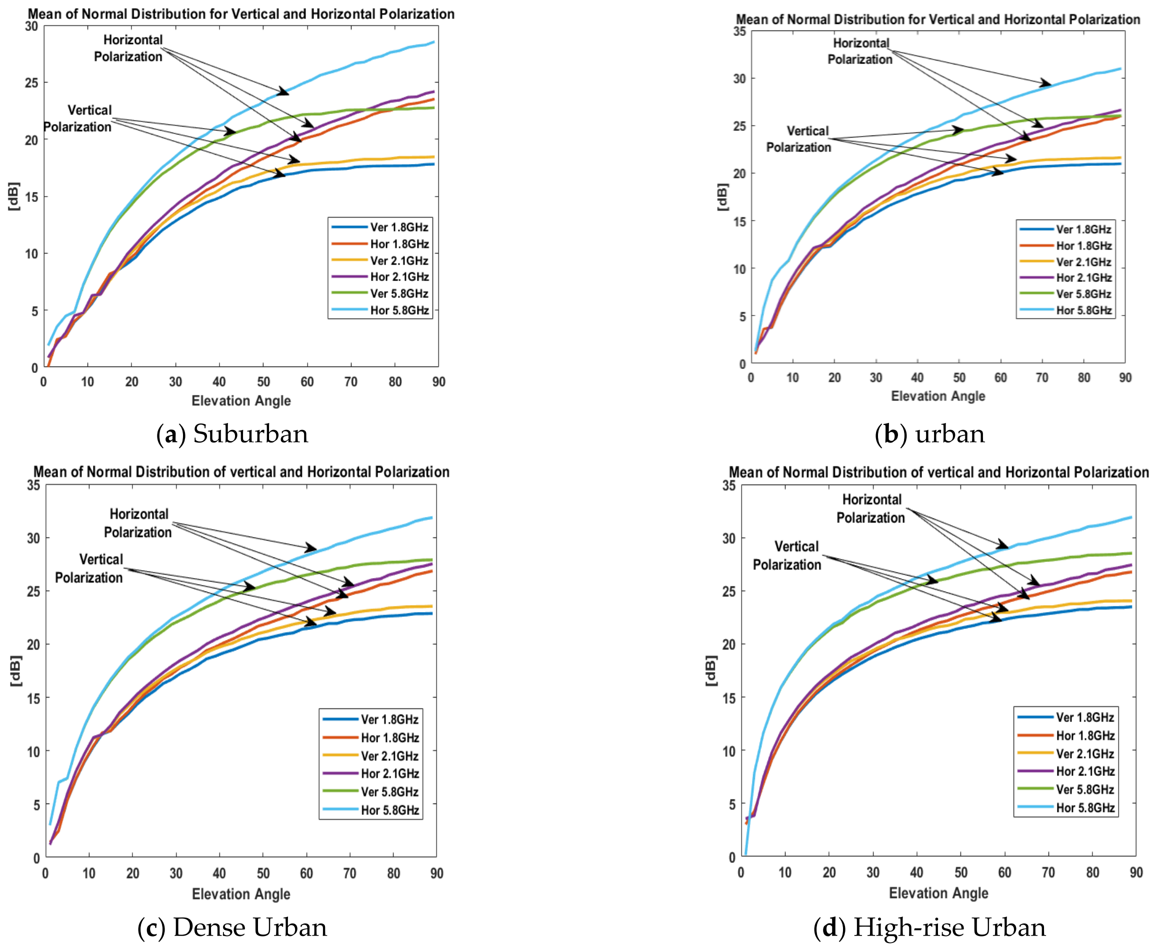

Figure 7. (**a**–**d**) Standard deviation of normal distribution for horizontal and vertical polarization at 1.8 GHz, 2.1 GHz, and 5.8 GHz for different environments for a range of elevation angles.

Table 3. Mean for vertical polarization at different frequencies.

Suburban		**100 m**	**200 m**	**300 m**	**400 m**	**500 m**
1.8 GHz	p_1	23.7216	24.0883	23.8048	23.7678	23.5960
	p_2	−29.9015	−36.7989	−36.9605	−31.5423	−34.1584
	p_3	22.2064	22.2152	22.2862	22.2410	21.3403
2.1 GHz	p_1	25.1339	25.2131	24.9089	24.6789	24.4703
	p_2	−32.2446	−32.6191	−31.6761	−29.4293	−28.6999
	p_3	29.2789	25.1215	23.2878	22.3367	21.3743
5.8 GHz	p_1	28.8010	28.9738	28.7539	28.6436	28.5876
	p_2	−30.8454	−29.2240	−28.5110	−27.0202	−26.3835
	p_3	20.9991	18.5201	17.2056	16.7119	16.4857
Urban						
1.8 GHz	p_1	25.4228	26.5718	26.3567	26.2121	26.0853
	p_2	−2.9948	−15.0461	−21.0732	−26.0114	−26.2173
	p_3	23.9305	19.5814	17.3439	16.1217	15.5793
2.1 GHz	p_1	25.9287	27.0221	27.0222	26.8835	26.7900
	p_2	−3.3181	−15.4761	−17.9286	−19.9051	−23.0595
	p_3	22.5635	18.3154	16.8960	15.9480	15.3296
5.8 GHz	p_1	29.6679	31.0097	31.2253	31.1271	30.9798
	p_2	−19.9921	−3.8644	−12.0476	−12.5775	−13.5733
	p_3	17.2139	14.6677	13.7547	13.1230	12.6010
Dense Urban						
1.8 GHz	p_1	25.2118	28.2947	28.7122	28.5990	28.6188
	p_2	10.1286	−9.2078	−11.0606	−19.5715	−19.9987
	p_3	22.4716	19.1733	17.9622	16.4188	16.0471
2.1 GHz	p_1	25.4447	28.9292	29.3238	29.3915	29.3611
	p_2	1.5633	−5.1620	−14.5809	−18.3496	−19.6060
	p_3	19.8798	18.6637	17.0602	16.3199	15.8336
5.8 GHz	p_1	29.7586	33.1945	33.5504	33.5410	33.4350
	p_2	36.7097	16.3986	4.3173	0.6839	−4.1420
	p_3	17.5222	16.0942	14.6104	13.8227	13.1878
High-Rise Urban						
1.8 GHz	p_1	20.3463	27.4242	28.4428	28.7052	28.8546
	p_2	17.5012	4.0327	0.3840	−8.1527	−7.1619
	p_3	14.0465	14.1650	13.1850	12.2438	12.1136
2.1 GHz	p_1	21.0427	27.9894	29.0438	29.3998	29.4792
	p_2	22.0963	4.9665	2.1906	−2.9504	−5.6475
	p_3	13.8743	13.5637	12.7458	12.1928	11.7493
5.8 GHz	p_1	24.1529	31.0331	32.2939	32.7668	32.9584
	p_2	−14.2152	−19.4081	−22.4160	−21.4092	−22.5993
	p_3	6.2512	7.7838	7.6857	7.7134	7.5998

Table 4. Means for horizontal polarization at different frequencies.

Suburban		**100 m**	**200 m**	**300 m**	**400 m**	**500 m**
1.8 GHz	p_1	35.6745	38.3942	38.8261	39.2372	39.1544
	p_2	−18.1666	−23.6267	−28.3137	−20.8376	−30.5913
	p_3	57.6867	54.1762	51.9193	52.0133	50.4158
2.1 GHz	p_1	31.0113	36.4189	37.9059	38.3037	38.4629
	p_2	15.1345	17.0104	19.3257	14.9433	8.1047
	p_3	32.2843	34.7100	35.0109	34.1919	33.3575
5.8 GHz	p_1	36.2385	39.8708	40.4364	40.7366	41.0820
	p_2	−19.4166	−6.3016	−13.2586	−14.0001	−8.0419
	p_3	32.9455	35.0245	33.8670	33.5594	34.004
Urban						
1.8 GHz	p_1	30.7810	30.9439	37.3921	37.6546	37.9306
	p_2	17.4879	17.4879	10.6488	1.9634	−2.0582
	p_3	34.8856	35.3342	35.9805	34.6766	34.1562
2.1 GHz	p_1	31.0113	36.4189	37.9059	38.3037	38.4629
	p_2	15.1345	17.0104	19.3257	14.9433	34.1919
	p_3	32.2843	34.7100	35.0109	8.1047	33.3575
5.8 GHz	p_1	34.0326	39.2117	40.5478	41.0711	41.3309
	p_2	35.0653	39.9744	25.1888	26.9476	27.1345
	p_3	24.0709	26.5295	26.0679	25.9490	25.8098
Dense Urban						
1.8 GHz	p_1	28.0617	35.4410	38.0706	38.9074	39.5604
	p_2	23.2720	20.3020	26.1260	14.1716	13.6524
	p_3	27.9972	31.4166	33.1805	32.4072	32.5977
2.1 GHz	p_1	25.4447	28.9292	29.3238	29.3915	29.3611
	p_2	1.5633	−5.1620	−14.5809	−18.3496	−19.6060
	p_3	19.8798	18.6637	17.0602	16.3199	15.8336
5.8 GHz	p_1	32.2079	39.3991	41.5958	42.5604	42.8968
	p_2	53.9679	55.2319	48.7093	48.0354	40.7040
	p_3	21.2534	24.7038	25.1447	25.2794	24.7796
High-Rise Urban						
1.8 GHz	p_1	21.3318	32.2853	35.5201	36.7368	37.5098
	p_2	23.1789	29.8386	37.4605	26.3565	27.7044
	p_3	15.8443	21.6186	23.4886	23.1616	23.4518
2.1 GHz	p_1	22.0077	32.7059	35.9666	37.4077	38.0281
	p_2	27.8509	30.2808	39.9798	36.0752	32.6578
	p_3	15.5492	20.4536	22.5132	22.9589	22.8287
5.8 GHz	p_1	24.9204	34.9199	38.0406	39.4709	40.2425
	p_2	−12.0049	−2.3964	2.7190	7.4398	7.3907
	p_3	7.05918	12.0028	13.7630	14.6158	14.9451

Table 5. Standard deviations for vertical/horizontal polarization in different.

Environment	s_1	s_2
Suburban	0.00112	4.944
Urban	0.00136	4.936
Dense urban	0.00141	4.931
High-rise urban	0.001591	4.927

Table 5, meanwhile, focuses on the parameters s_1 and s_2, which signify the standard deviations associated with our findings. A noteworthy outcome of our analysis is the discovery that the s_1 and s_2 parameters exhibit remarkable consistency, showing no significant variation across a spectrum of conditions, including different altitudes, polarizations, and frequencies tested. This consistency allows us to derive the standard deviation from a single, unified equation, greatly simplifying the overall calculation process. For additional frequencies within the range of 2 and 6 GHz, we can obtain values through interpolation, utilizing the parameters presented in Tables 3–5. It is crucial to apply these parameters with the specified precision in decimal points in all calculations to ensure accuracy.

The implications of these findings are expected to be significant, particularly in the context of evaluating additional shadowing path loss. Our work takes into account the complex interactions associated with various frequencies, altitudes, polarizations, and environmental contexts. Ultimately, this extensive experimentation has culminated in the development of a comprehensive and refined solution for the UAV channel model, specifically attuned for the unique challenges of an Indian metropolitan area. This model is particularly focused on radio frequency (RF) planning at low altitudes, effectively addressing the intricate nuances introduced by differing frequencies and polarizations, thereby enhancing the planning capabilities vital for urban environments.

4.3. Shadowing Path Loss

As discussed earlier, the shadowing path loss for the environment was given by normal distribution with mean μ and standard deviation σ (Equations (7) and (8)). The path loss is given by

$$Ls = normrand\left(\frac{p_1\theta + p_2}{\theta + p_3},\ s_1\theta + s_2\right) \tag{9}$$

5. Proposed Channel Model

As discussed in previous sections, the path loss for LoS scenario is calculated using free space path loss (FSPL), and for NLoS scenarios, additional shadowing loss is included, formulated in terms of the normal distribution. The total path loss for the proposed channel model is

$$L = L_{FSPL} + L_A + L_{ex} \tag{10}$$

where L_{FSPL} is the average free space path loss, which is determined by the distance and frequency. L_A stands for the antenna loss. L_{ex} stands for the additional shadowing loss, which accounts for obstruction between transmitter and receiver as well as additional loss due to environmental effects.

5.1. Free Space Path Loss

The free space path loss (FSPL), described as a function of the elevation angle between UAV and receiver, is given by

$$L_{FSPL} = 20log\frac{\Delta h}{\sin\theta} + 20logf\ -\ 27.55 \tag{11}$$

where $\Delta h = h_{UAV} - h_r$ is the height difference between transmitter (UAV) (h_{UAV}) and receiver (hr), measured in kilometers, and f is the frequency, measured in MHz.

5.2. Antenna Loss

As per ITU-R P.1336-1 [41], the relative gain G(θ) of the antenna with respect to the isotropic antenna (dBi) can be given as

$$G(\theta) = \begin{matrix} G_0 - 12\left(\frac{\theta}{\theta_3}\right)^2 & 0 \leq \theta < \theta_3 \\ G_0 - 12 -\ 10log\frac{\theta}{\theta_3} & \theta_3 \leq \theta < 90 \end{matrix} \tag{12}$$

where $\theta_3 = 107.6\ x10^{-0.1\ x\ Go}$; G_0 is the maximum value of gain in or near the horizontal plane in dBi; θ is the absolute elevation angles relative to the maximum gain angle in degrees; θ_3 is the 3 dB beam width at the vertical plane in degrees. The path loss due to transmitting and receiving antennas is calculated by

$$L_A = -2 * G(\theta) \tag{13}$$

5.3. Excess Path Loss (L_{ex})

The excessive path loss for NLoS communication can be obtained from the probability of line-of-sight communication.

$$L_{ex} = L_s + 20\log(1 - P_{LoS}) \tag{14}$$

where L_s is the additional path loss or shadowing loss due to shadowing when the wedges obstruct the line-of-sight ray.

5.4. Path Loss

The path loss represented by Equation (6) is

$$L = L_{FSPL} + L_A + L_{ex}$$

By substituting values from Equations (9), (11)–(14), the path loss can be represented by

$$L = 20log\frac{(h_{uav} -\ h_r)}{sin\theta} + A - 20log\frac{\theta}{\theta_3} + Ls + 20\log(1 - P_{LoS}) \tag{15}$$

where

$$A = 20logf - 51.55 - 2G_0 \tag{16}$$

5.5. Proposed Model Analysis

The analysis includes the simulation of proposed path loss in four different environments at varying frequencies and altitudes, considering elevation angles as depicted in Figures 8 and 9. The findings provide a detailed analysis of path loss across various environments at a frequency of 5.8 GHz, specifically at a UAV altitude of 200 m. As shown in Figure 8a, the results reveal that the suburban environment experiences the lowest level of path loss, indicative of more favorable communication conditions. In contrast, the dense urban environment is characterized by significantly higher path loss, attributed to the greater density of buildings and obstacles that contribute to increased signal attenuation and shadowing.

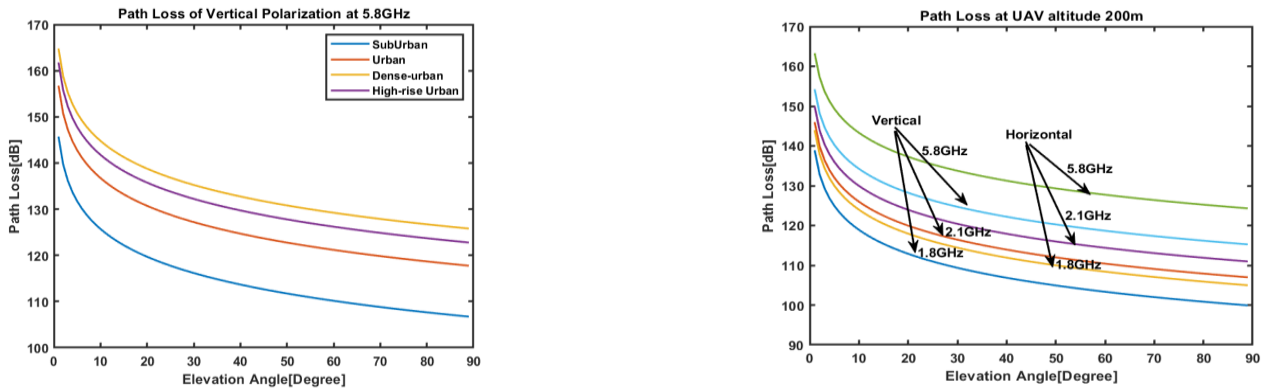

(**a**) (**b**)

Figure 8. Proposed model path loss for (**a**) different environments at frequency 5.8 GHz and altitude 200 m and (**b**) dense urban environments at different frequencies and polarization at altitude 200 m.

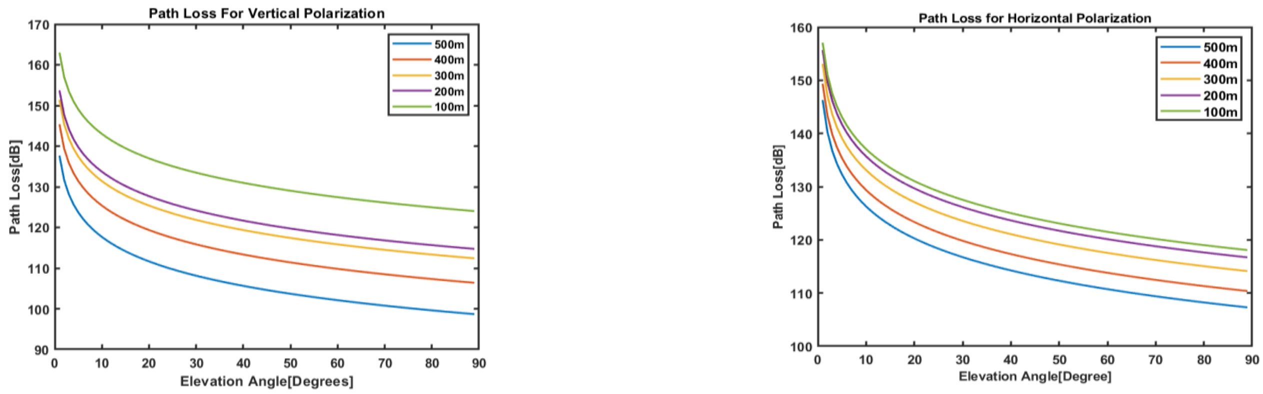

(**a**) (**b**)

Figure 9. (**a**,**b**) Proposed model path loss for dense urban environment at UAV altitude 100–500 m at frequency 5.8 GHz for vertical and horizontal polarization, respectively.

This trend is consistent across additional frequencies of 1.8 GHz and 2.1 GHz, observed at varying altitudes. To further understand the behavior of path loss in the dense urban setting, simulations were conducted for 1.8 GHz, 2.1 GHz, and 5.8 GHz, focusing on both vertical and horizontal polarization of the signals. Figure 8b illustrates that as frequency increases, there is a corresponding rise in path loss for both types of polarization, highlighting the challenges posed by higher frequency signals in urban landscapes.

In addition, this study examines the relationship between the altitude of the UAV and its impact on the path loss. Figure 9a,b depict a strong correlation: as the UAV's altitude increases, resulting in a notable decrease in overall path loss due to increase in line-of-sight communication between transmitter and receiver. This finding provides valuable insight into how variations in altitude can significantly influence the effectiveness of communication systems, particularly in urban environments where obstructions are prevalent. Overall, this comprehensive analysis deepens our understanding of the dynamics affecting path loss in various scenarios.

6. Proposed Model Validation

The proposed model is designed to enhance the simulation of coverage estimation for deploying 5G services in the bustling metropolitan cities of India. This model seeks to streamline the computational process involved in simulations, making it quicker and more efficient. The accuracy of any channel model is fundamentally tied to the mathematical assumptions it employs. For instance, if the actual layout of buildings in the target area diverges significantly from the assumptions made by the model, the predictions regarding signal behavior and coverage may suffer. To provide a robust validation of the proposed channel model presented in this paper, path loss comparisons were conducted against established models: Model 1 [27] and Model 2 [31] are specifically designed for dense urban environments. The simulation parameters detailed in Table 6 are utilized for validation.

Table 6. Model parameters.

Model Parameter	Value
Frequency	5.8 GHz
h_{UAV}	200 m
h_r	2 m
G_o	2.15
θ_3	67

The results shown in Figure 10 demonstrate a close alignment between the existing model and the proposed model. Notably, the existing models do not account for the effect of polarization on path loss. Furthermore, other models' scenarios are validated against the estimates found in [27], where a similar close correlation is also observed. The close alignment of the proposed model with the existing model ensures that the mathematical framework of the model effectively reproduces key aspects of path loss and the propagation characteristics essential for successful 5G deployment.

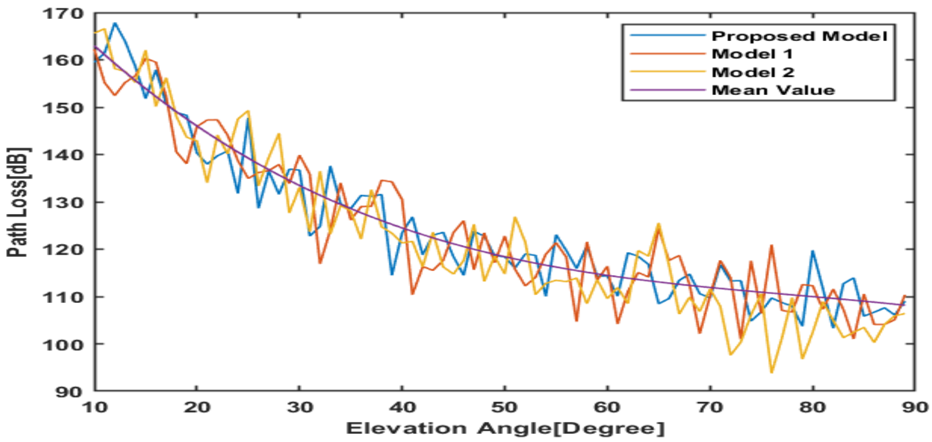

Figure 10. Proposed model vs other models.

7. Conclusions

An elevation-based shadowing statistical model was developed for low-altitude UAV (unmanned aerial vehicle) channels in various environments, including suburban, urban, dense urban, and high-rise urban settings. This model, formulated as a function of elevation angle, covers a frequency range from 1.8 GHz to 6 GHz and altitudes up to 500 m, considering both vertical and horizontal polarization. The shadowing path loss for non-line-of-sight (NLoS) conditions is presented with elevation angle. It is a valuable tool for radio network planning to support the expansion of 5G communication in Indian metropolitan cities. Based on extensive simulations, the model provides an efficient formula that minimizes computational time while maintaining a strong correlation with existing air-to-ground models. Additionally, it analyzes the impact of frequency and UAV height adjustments, offering a structured framework for determining optimal UAV altitudes, ultimately maximizing ground coverage and enhancing communication performance. Derived from extensive simulations, the model provides a simplified formula for implementation, effectively reducing computational time. Notably, it demonstrates a strong correlation with other air-to-ground models. Furthermore, the model analyzes the effects of frequency and UAV height adjustments, providing a straightforward framework for determining the optimal UAV altitude to maximize ground coverage.

Author Contributions: Conceptualization, A.K.P. and R.D.J.; methodology, A.K.P.; software, A.K.P.; validation, A.K.P.; formal analysis, A.K.P. and R.D.J.; investigation, A.K.P. and R.D.J.; resources, A.K.P.; data curation, A.K.P.; writing—original draft, A.K.P.; writing—review and editing, A.K.P. and R.D.J.; visualization, A.K.P. and R.D.J. All authors have read and agreed to the published version of the manuscript.

Funding: This research received no external funding.

Data Availability Statement: The contributions made in this study are documented within the article. For any additional inquiries, please direct your questions to the corresponding author.

Acknowledgments: This work was supported by the College of Engineering, Pune.

Conflicts of Interest: Authors declare that there are no known conflicts of interest related to this study.

References

1. Tyokighir, S.S.; Mom, J.; Ukhurebor, K.E.; Igwue, G. New developments and trends in 5G technologies: Applications and concepts. *Bull. Electr. Eng. Inform.* **2024**, *13*, 254–263. [CrossRef]
2. What is 5G? How will it transform our world? Available online: https://www.ericsson.com/en/5g (accessed on 30 November 2023).
3. Amponis, G.; Lagkas, T.; Zevgara, M.; Katsikas, G.; Xirofotos, T.; Moscholios, I.; Sarigiannidis, P. Drones in B5G/6G Networks as Flying Base Stations. *Drones* **2022**, *6*, 39. [CrossRef]
4. Rolly, R.M.; Malarvezhi, P.; Lagkas, T.D. Unmanned aerial vehicles: Applications, techniques, and challenges as aerial base stations. *Int. J. Distrib. Sens. Netw.* **2022**, *18*, 1–9. [CrossRef]
5. Masaoka, R.; Tran, G.K.; Nakazato, J.; Sakaguchi, K. The Future of Flying Base Stations: Empirical and Numerical Investigations of mmWave-Enabled UAVs. *Future Internet* **2024**, *16*, 5. [CrossRef]
6. Mohsan, S.A.H.; Othman, N.Q.H.; Li, Y.; Alsharif, M.H. Unmanned aerial vehicles (UAVs): Practical aspects, applications, open challenges, security issues, and future trends. *Intell. Serv. Robot.* **2023**, *16*, 109–137. [CrossRef]
7. Ghamari, M.; Rangel, P.; Mehrubeoglu, M.; Tewolde, G.S.; Sherratt, R.S. Unmanned Aerial Vehicle Communications for Civil Applications: A Review. *IEEE Access* **2022**, *10*, 102492–102531. [CrossRef]
8. Shah, A.F.M.S. Architecture of Emergency Communication Systems in Disasters through UAVs in 5G and Beyond. *Drones* **2023**, *7*, 25. [CrossRef]
9. Khawaja, W.; Guvenc, I.; Matolak, D.W.; Fiebig, U.-C.; Schneckenburger, N. Survey of air-to-ground propagation channel modelling for unmanned aerial vehicles. *IEEE Commun. Surv. Tutor.* **2019**, *21*, 2361–2391. [CrossRef]
10. Matolak, D.W.; Sun, R. Air-ground channel characterization for unmanned aircraft systems-part i: Methods, measurements, and models for over-water settings. *IEEE Trans. Veh. Technol.* **2016**, *66*, 26–44. [CrossRef]
11. Dhillon, H.S. Downlink coverage analysis for a finite 3-d wireless network of unmanned aerial vehicles. *IEEE Trans. Commun.* **2017**, *65*, 4543–4558.
12. Sun, R.; Matolak, D.W. Air-ground channel characterization for unmanned aircraft systems-part ii: Hilly and mountainous settings. *IEEE Trans. Veh. Technol.* **2017**, *66*, 1913–1925. [CrossRef]
13. Matolak, D.W.; Sun, R. Air-ground channel characterization for unmanned aircraft systems-part iii: The suburban and near urban environments. *IEEE Trans. Veh. Technol.* **2017**, *66*, 6607–6618. [CrossRef]
14. Sun, R.; Matolak, D.W.; Rayess, W. Air-ground channel characterization for unmanned aircraft systems—Part IV: Airframe shadowing. *IEEE Trans. Veh. Technol.* **2017**, *66*, 7643–7652. [CrossRef]

15. Schneckenburger, N.; Jost, T.; Shutin, D.; Walter, M.; Thiasiriphet, T.; Schnell, M.; Fiebig, U.C. Measurement of the L-band air-to-ground channel for positioning applications. *IEEE Trans. Aerosp. Electron. Syst.* **2016**, *52*, 2281–2297. [CrossRef]
16. Takizawa, K.; Kagawa, T.; Lin, S.; Ono, F.; Tsuji, H.; Miura, R. C-band aircraft-to-ground (A2G) radio channel measurement for unmanned aircraft systems. In Proceedings of the International Symposium on Wireless Personal Multimedia Communications (WPMC), Sydney, Australia, 7–10 September 2014; pp. 754–758.
17. Lyu, Y.; Wang, W.; Sun, Y.; Yue, H.; Chai, J. Low-Altitude UAV Air-to-Ground Multilink Channel Modeling and Analysis at 2.4 and 5.9 GHz. *IEEE Antennas Wirel. Propag. Lett.* **2023**, *22*, 2135–2139. [CrossRef]
18. Qiu, Z.; Chu, X.; Calvo-Ramirez, C.; Briso, C.; Yin, X. Low Altitude UAV Air-to-Ground Channel Measurement and Modeling in Semiurban Environments. *Wirel. Commun. Mob. Comput.* **2017**, *2017*, 1587412. [CrossRef]
19. Lyu, Y.; Wang, W.; Chen, P. Fixed-Wing UAV Based Air-to-Ground Channel Measurement and Modeling at 2.7 GHz in Rural Environment. *IEEE Trans. Antennas Propag.* **2024**, *1*. [CrossRef]
20. Cui, Z.; Briso-Rodríguez, C.; Guan, K.; Zhong, Z.; Quitin, F. Multi-frequency air-to-ground channel measurements and analysis for UAV communication systems. *IEEE Access* **2020**, *8*, 110565–110574. [CrossRef]
21. Zhang, X.; He, R.; Yang, M.; Ai, B.; Wang, S.; Li, W.; Sun, W.; Li, L.; Huang, P.; Xue, Y. Measurements and modeling of large-scale channel characteristics in subway tunnels at 1.8 and 5.8 GHz. *IEEE Antennas Wirel. Propag. Lett.* **2023**, *22*, 561–565. [CrossRef]
22. Yang, M.; Ai, B.; He, R.; Ma, Z.; Zhong, Z. Vehicle-to-vehicle channel characteristics in intersection environment. In Proceedings of the 2022 IEEE International Conference on Communications Workshops (ICC Workshops), Seoul, Republic of Korea, 16–20 May 2022; pp. 1124–1129.
23. Li, Y.; Cheng, X. Modelling and simulation for UAV-aided vehicular MIMO communication channels. *IET Commun.* **2019**, *13*, 3044–3051. [CrossRef]
24. Jiang, H.; Zhang, Z.; Wu, L.; Dang, J. Three-dimensional geometry-based UAV MIMO channel modeling for A2G communication environments. *IEEE Commun. Lett.* **2018**, *22*, 1438–1441. [CrossRef]
25. Cheng, X.; Li, Y. A 3-D geometry-based stochastic model for UAV-MIMO wideband nonstationary channels. *IEEE Internet Things J.* **2018**, *6*, 1654–1662. [CrossRef]
26. Yi, P.; Zhu, L.; Xiao, Z.; Zhang, R.; Han, Z.; Xia, X.G. 3-D Positioning and Resource Allocation for Multi-UAV Base Stations Under Blockage-Aware Channel Model. *IEEE Trans. Wirel. Commun.* **2024**, *23*, 2453–2468. [CrossRef]
27. Al-Hourani, A.; Kandeepan, S.; Jamalipour, A. Modeling air-to-ground path loss for low altitude platforms in urban Environments. In Proceedings of the IEEE Global Communications Conference, Austin, TX, USA, 8–12 December 2014; pp. 2898–2904.
28. Al-Hourani, A. On the Probability of Line-of-Sight in Urban Environments. *IEEE Wirel. Commun. Lett.* **2020**, *9*, 1178–1181. [CrossRef]
29. Akram, A.L.; Chandrasekharan, S.; Kaandorp, G.; Glenn, W.; Jamalipour, A.; Kandeepan, S. Coverage and rate analysis of Aerial Base Station. *IEEE Trans. Aerosp. Electron. Syst.* **2016**, *52*, 3077–3081.
30. Al-Hourani, A.; Kandeepan, S.; Lardner, S. Optimal LAP Altitude for Maximum Coverage. *IEEE Wirel. Commun. Lett.* **2014**, *3*, 569–572. [CrossRef]
31. Safwat, N.E.; Newagy, F.; Hafez, I.M. Air-to-ground channel model for UAVs in dense urban environments. *IET Commun.* **2020**, *14*, 1016–1021. [CrossRef]
32. Holis, J.; Pechac, P. Elevation Dependent Shadowing Model for Mobile Communications via High Altitude Platforms in Built-Up Areas. *IEEE Trans Antennas Propag.* **2008**, *56*, 1078–1084. [CrossRef]
33. Patel, A.K.; Joshi, R.D. Area Coverage Analysis of Low Altitude UAV Bases Station using Statistical Channel Model. In Proceedings of the International Conference on Signal and Information Processing (IConSIP), Pune, India, 26–27 August 2022; pp. 1–6.
34. Patel, A.K.; Joshi, R.D. Coverage Estimation Using Probabilistic Line-of-Sight Model for Unmanned Aerial Vehicle Communication. In Proceedings of the UASG 2021: Wings 4 Sustainability UASG Lecture Notes in Civil Engineering, International Conference on Unmanned Aerial System in Geomatics, Roorkee, India, 2–4 April 2021; Jain, K., Mishra, V., Pradhan, B., Eds.; Springer: Berlin/Heidelberg, Germany, 2023; Volume 304, pp. 533–544.
35. Kumar, M.; Arti, M.K. A simple characterization of UAV communication systems. *Sādhanā* **2022**, *47*, 210. [CrossRef]
36. ITU-R. *Recommendation P.1410-5 Propagation Data and Prediction Methods for The Design of Terrestrial Broadband Millimetric Radio Access Systems*; P Series; Radiowave Propagation; International Telecommunication Union: Geneva, Switzerland, 2005.
37. Kouyoumjian, R.G.; Pathak, P.H. A uniform geometrical theory of diffraction for an edge in a perfectly conducting surface. *Proc. IEEE* **1974**, *62*, 1448–1461. [CrossRef]
38. Luebbers, R. Finite conductivity uniform GTD versus knife edge diffraction in prediction of propagation path loss. *IEEE Trans. Antennas Propag.* **1984**, *32*, 70–76. [CrossRef]
39. Brugarolas-Ortiz, E.; Rodríguez-Rodríguez, I.; Rodríguez, J.-V.; Juan-Llácer, L.; Pardo-Quiles, D. Using the Uniform Theory of Diffraction to Analyze Radio Wave Propagation along Urban Street Canyons for Device-to-Device Communication. *Electronics* **2023**, *12*, 593. [CrossRef]

40. ITU-R. *Recommendation P.526-14 Propagation by Diffraction, P Series, Radiowave Propagation*; International Telecommunication Union: Geneva, Switzerland, 2018.
41. ITU-R. *Recommendation F.1336-1 Reference Radiation Patterns of Omnidirectional, Sectoral and other Antennas in Point-To-Multipoint Systems for Use in Sharing Studies in the Frequency Range from 1 GHz to About 70 GHz*; International Telecommunication Union: Geneva, Switzerland, 2000.